From stationary annular rings to rotating Bessel beams

Angela Dudley[1],[2],* and Andrew Forbes[1],[2]

[1]CSIR National Laser Centre, P.O. Box 395, Pretoria 0001, South Africa
[2]School of Physics, University of KwaZulu-Natal, Private Bag X54001, Durban 4000, South Africa
*Corresponding author: adudley@csir.co.za

In this work we use a phase-only spatial light modulator (SLM) to mimic a ring-slit aperture, containing multiple azimuthally varying phases at different radial positions. The optical Fourier transform of such an aperture is currently known and its intensity profile has been shown to rotate along its propagation axis. Here we investigate the near-field of the ring-slit aperture and show, both experimentally and theoretically, that although the near-field possesses similar attributes to its Fourier transform, its intensity profile exhibits no rotation as it propagates.   © 2012 Optical Society of America

OCIS codes: 090.1995, 070.6120, 070.3185, 050.4865.

1. INTRODUCTION

Currently, there is a large amount of literature dedicated to fields carrying orbital angular momentum (OAM). This ranges across Laguerre–Gaussian beams [1], Bessel–Gauss beams [2], and Airy beams [3], all of which carry an OAM of $l\hbar$ per photon and have an azimuthal angular dependence of $\exp(il\phi)$ [1,4–6], where l is the unbounded azimuthal mode index and ϕ is the azimuthal angle. Fields carrying OAM offer versatile applications. Some of these applications range from using such fields to transfer OAM for the rotation of trapped particles [5] to the entanglement of OAM in parametric down-conversion [6]. The fact that they offer an unbounded state space provides a larger bandwidth for quantum cryptography [7,8].

We are mainly interested in higher-order non-diffracting Bessel beams as a form of optical field possessing OAM and of particular interest is the generation of superimposed higher-order Bessel beams. One can superimpose higher-order Bessel beams so as to produce a field which either has or does not have a global OAM. In the case of generating a superimposed higher-order Bessel beam, such that there is no global OAM, a rotation in the field's intensity profile as it propagates is evident [9–11]. Such superpositions can be generated by illuminating Durnin's ring-slit aperture [12] with multiple azimuthal phase components at varying radial distances [9], or by encoding a spatial light modulator (SLM) with a single ring-slit hologram [10], or by illuminating an axicon with a superposition of Laguerre–Gaussian beams [13].

In this paper we, theoretically and experimentally, investigate both the near- and far-field intensity profiles of the ring-slit aperture. Since superpositions of Bessel beams are frequently used in optical tweezers, knowledge of the structure of the field at planes, other than its Fourier plane, is imperative. We show that even though the intensity maxima, present in the far-field as $2l$ "petals," arranged on the circumference of a ring [9], are also present in the near-ring-slit field, the angular rotation of the intensity profile, however, does not exist in both the near- and far-field regions. It is well known that the far-field intensity profile rotates as it propagates [9–11] and we show, both theoretically and experimentally, that this is not the case

in the near-field, due to the fact that the longitudinal wave vectors all propagate in the same direction (and do not overlap one another) in the near-field, but in differing directions (overlapping one another) in the far-field.

2. THEORY

In this work we implement Durnin's ring-slit aperture experiment [12] and encode a digital ring-slit hologram onto a SLM and illuminate it with an expanded Gaussian beam. We divide the ring-slit aperture into two ring-slits and encode each with an azimuthally varying phase. A schematic of the setup is given in Fig. 1, where the regions of interest, propagating after the ring-slit aperture, are planes P_1 (the near field), the region P_2 (the transition region from near- to far-field) and region P_3 (the far-field).

The ring-slit aperture, has the following transmission function

$$t(r,\phi) = \begin{cases} \exp(il\phi) & R_1 - \frac{\Delta}{2} \le r \le R_1 + \frac{\Delta}{2} \\ \exp(-il\phi) & R_2 - \frac{\Delta}{2} \le r \le R_2 + \frac{\Delta}{2}, \\ 0 & \text{elsewhere} \end{cases} \tag{1}$$

and apart from being illustrated in Fig. 1, is also represented in Fig. 2. R_1 and R_2 are the radii of each of the two ring-slits, respectively, and Δ is the width of each ring-slit (we have chosen the widths of the two ring-slits to be equal). ϕ is the azimuthal angle and l is the azimuthal mode index.

Since the field illuminating the ring-slit aperture is an expanded Gaussian beam and the ring-slits are extremely thin (of the order of micrometers), the optical field within the rings-slit can be described by a plane-wave, $\exp(i(k_z z - \omega t))$. k_z is the longitudinal wavenumber, z is the propagation axis and the time varying component, ωt, can be neglected as the plane-wave field is uniform across the entire $x - y$ plane, at any instant in time. The field produced at the ring-slit aperture (i.e., at the plane P_1 where $z = z_0$), is represented as
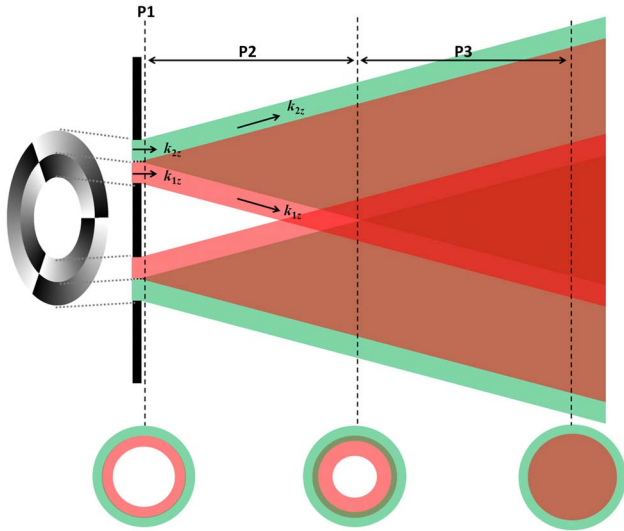
Fig. 1. (Color online) Schematic of the generation of the annular field, propagating from near- (P_1) to far-field (P_3). The green (red) rays denote the rays originating from the outer (inner) ring-slit. The three rings (at the bottom of the schematic) aid the illustration, as to how the annular fields overlap and become completely indistinguishable as the propagation from the aperture increases.

$$A^{P_1}(r,\phi,z_0) = \begin{cases} \exp(il\phi)\exp(ik_{1z}z_0) & R_1 - \frac{\Delta}{2} \le r \le R_1 + \frac{\Delta}{2} \\ \exp(-il\phi)\exp(ik_{2z}z_0) & R_2 - \frac{\Delta}{2} \le r \le R_2 + \frac{\Delta}{2} \\ 0 & \text{elsewhere} \end{cases} \tag{2}$$

k_{1z} and k_{2z} are the longitudinal wavenumbers, defined as $k_{1z} = k\cos\alpha_1$ and $k_{21z} = k\cos\alpha_1$, where $k = 2\pi/\lambda$ and α is the opening angle of the cone on which the wave vectors (produced by each of the two ring-slits) propagate.

A simple annular field, containing no azimuthally varying phase factors, is expressed as

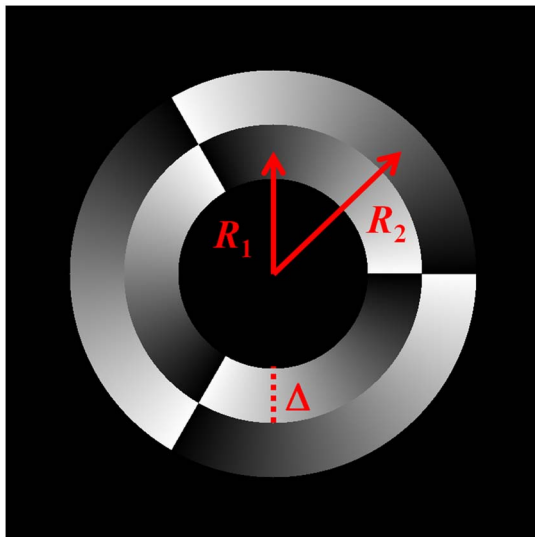$$A^{\text{Ring}}(r) = \exp\left(\left(\frac{-(r-R_0)}{\Delta/2}\right)^n\right) \tag{3}$$

Fig. 2. (Color online) Density plot of the transmission function described in Eq. (1) for an azimuthal mode index of $l = 3$.

and is depicted graphically in Fig. 3. R_0 denotes the radius of the ring-slit, Δ is the width of the ring-slit, and n assigns the steepness (or gradient) of the edges of the ring-slit.

The ring-slit aperture that we are considering, consists of two ring-slits of differing radii, and by taking into account that the optical field is a linear system, the two annular fields are additive, resulting in the overall ring-slit field, in the near-field (P_1), been written as

$$\begin{aligned} A^{P_1}(r,\phi,z_0) &= A^{\text{Ring1}}(r)\exp(il\phi)\exp(ik_{1z}z_0) \\ &\quad + A^{\text{Ring2}}(r)\exp(-il\phi)\exp(ik_{2z}z_0) \\ &= \exp\left(\left(\frac{-(r-R_1)}{\Delta/2}\right)^n\right)\exp(il\phi)\exp(ik_{1z}z_0) \\ &\quad + \exp\left(\left(\frac{-(r-R_2)}{\Delta/2}\right)^n\right)\exp(-il\phi)\exp(ik_{2z}z_0). \end{aligned} \tag{4}$$

Since the two ring-slits are arbitrary thin and close to one another, we can assume their radii to be equivalent, i.e., $R_1 = R_2 = R_0$, resulting in the field simplifying to

$$\begin{aligned} A^{P_1}(r,\phi,z_0) &= \exp\left(\left(\frac{-(r-R_0)}{\Delta/2}\right)^n\right)(\exp(il\phi)\exp(ik_{1z}z_0) \\ &\quad + \exp(-il\phi)\exp(ik_{2z}z_0)). \end{aligned} \tag{5}$$

The intensity of the ring-slit field is determined with the following relationship: $I = AA^*$, resulting in

$$\begin{aligned} I^{P_1}(r,\phi,z_0) &= 4\cos^2\left(\frac{k_{1z}z_0 - k_{2z}z_0 + 2l\phi}{2}\right) \\ &\quad \times \left(\cosh\left(\frac{2(r-R_0)}{\Delta}\right) - \sinh\left(\frac{2(r-R_0)}{\Delta}\right)\right)^{2n}. \end{aligned} \tag{6}$$

The intensity profile for the ring-slit field, given above in Eq. (6), illustrates that it is modulated in the azimuthal coordinate, ϕ, by the function $\cos^2(2l\phi)$. Therefore, the number of intensity maxima and minima, arranged on the circumference of the ring-slit, is twice the azimuthal mode index, l.

The angular rotation, experienced by the intensity profile, as the ring-slit field propagates in the near-field (P_1) along the z-axis, is then given by
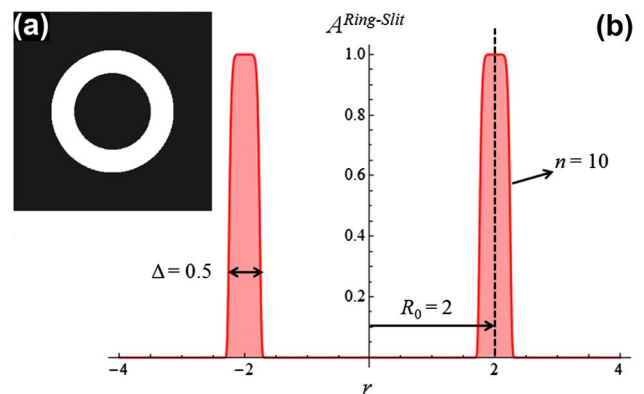

Fig. 3. (Color online) (a) Density plot and (b) cross-sectional plot of the ring-slit aperture described in Eq. (3) for the following parameters: ring-slit radius, $R_0 = 2$, ring-slit width, $\Delta = 0.5$, and gradient, $n = 10$ (the units are arbitrary).

$$\frac{d\phi}{dz_0} = \frac{k_{2z} - k_{1z}}{2l}. \qquad (7)$$

During the propagation of the ring-slit field, the longitudinal wave vectors, k_{1z} and k_{2z}, both propagate in the same direction, parallel to the z-axis, which is illustrated in Fig. 1. This results in no angular rotation existing, as the ring-slit field propagates,

$$\frac{d\phi}{dz_0} = 0. \qquad (8)$$

In determining the field in the region P_2, the region in which the field transitions from near- to far-field, the Fresnel diffraction integral of the field at the ring-slit aperture (Eq. (4)) can be calculated

$$A^{P_2}(r, \phi, z) = \frac{e^{ikz}}{i\lambda z} \int_0^{2\pi} \int_{R_1 - \frac{\Delta}{2}}^{R_2 + \frac{\Delta}{2}} A^{P1}(r, \phi, z)$$
$$\times \exp\left(i\frac{k}{2z}(r_1^2 + r^2 - 2rr_1\cos(\phi_1 - \phi))\right) r_1 dr_1 d\phi_1 \quad (9)$$

and is known to produce the Bessel–Gauss function [14,15]. Each of the two ring-slits (the inner having an azimuthal mode index of l and the outer, $-l$) will contribute to a Bessel–Gauss beam and the resulting superposition of the field in region P_2 can be described as

green and red rays. As the field propagates further towards the far-field (P_3), the overlap in the field, which consists of both ring-slit contributions, increases, resulting in the angular rotation becoming more evident.

To determine the far-field of the ring-slit aperture (P_3), whose transmission function $t(r, \phi)$ is given in Eq. (1), the Kirchoff–Huygens diffraction integral is used

$$A^{P_3}(r, \phi, z) = \frac{-i}{\lambda z} \int_0^{2\pi} \int_{R_1 - \frac{\Delta}{2}}^{R_2 + \frac{\Delta}{2}} t(r, \phi_1) \exp\left[i\frac{k}{2f}\left(1 - \frac{z}{f}\right)r_1^2\right]$$
$$\times \exp\left[-i\frac{krr_1}{f}\cos(\phi_1 - \phi)\right] r_1 dr_1 d\phi_1. \quad (12)$$

The contribution resulting from the inner and the outer ring-slits produces the following superposition, which describes the far-field of the ring-slit aperture [9]

$$A^{P_3}(r, \phi, z) = J_l(k_{1r}r) \exp(il\phi) \exp(ik_{1z}z)$$
$$+ J_{-l}(k_{2r}r) \exp(-il\phi) \exp(ik_{2z}z). \quad (13)$$

The intensity of the superimposed Bessel field is determined with the following relationship: $I = AA^*$, resulting in

$$I^{P_3}(r, \phi, z) \propto J_l^2(k_{1r}r) + J_{-l}^2(k_{2r}r)$$
$$+ 2J_l(k_{1r}r)J_{-l}(k_{2r}r) \cos(k_{1z}z - k_{2z}z + 2l\phi). \quad (14)$$

$$A^{P_2}(r, \phi, z) = A^{BG1}(r, \phi, z) + A^{BG2}(r, \phi, z)$$

$$= \left(\frac{1}{\sqrt{1 + \left(\frac{z}{z_r}\right)^2}}\right) \left(\begin{array}{l} \exp\left[i\left(kz - \frac{k_{1r}^2 z}{2k} - \Phi(z)\right) - \left(\frac{1}{\omega^2(z)} - \frac{ik}{2R(z)}\right)\left(r^2 + \left(\frac{k_{1r}z}{k}\right)^2\right) + ik_{1z}z + il\phi\right] J_l\left(\frac{k_{1r}r}{1 + i(z/z_r)}\right) + \\ \exp\left[i\left(kz - \frac{k_{2r}^2 z}{2k} - \Phi(z)\right) - \left(\frac{1}{\omega^2(z)} - \frac{ik}{2R(z)}\right)\left(r^2 + \left(\frac{k_{2r}z}{k}\right)^2\right) + ik_{2z}z - il\phi\right] J_{-l}\left(\frac{k_{2r}r}{1 + i(z/z_r)}\right) \end{array} \right). \quad (10)$$

The functions $\omega(z)$, $R(z)$ and $\Phi(z)$ denote the beam size, radius of curvature and Gouy phase, respectively, and take on the standard Gaussian beam propagation form. J_l is the lth order Bessel function and k_r denotes the transverse wavenumber, associated with each of the two Bessel beams, namely 1 and 2, and is determined as follows: $k_r = k \sin \alpha$.

Similarly the intensity in the region of P_2 can be determined by the following relationship: $I = AA^*$ (which has been neglected here, as the equation is very cumbersome) and the angular rotation results in

$$\frac{d\phi}{dz} \approx \frac{k_{2z} - k_{1z}}{2l}. \qquad (11)$$

The wave vectors in this region all point in opposite directions resulting in a non-zero rotation rate. However the only section of the field which experiences this angular rotation is the section which consists of the contributions from both ring-slits, which visually means: the sections which consist of both

Since the annular rings generating the superimposed Bessel beams are arbitrarily thin and close to one another, we can assume the transverse wavenumbers to be equivalent (i.e., $k_{1r} \sim k_{2r} = k_r$), resulting in $J_l(k_{1r}r) \sim J_l(k_{2r}r) = J_l(k_r r)$. By implementing the Bessel function identity, $J_{-l}(k_{2r}r) = (-1)^l J_l(k_{2r}r)$, the intensity in Eq. (14) can be simplified to produce

$$I^{P_3}(r, \phi, z) \propto 2J_l^2(k_r r)((-1)^l + 1$$
$$+ 2(-1)^l \cos(k_{1z}z - k_{2z}z + 2l\phi)). \quad (15)$$

The intensity profile for the superimposed Bessel beams, given above in Eq. (15), illustrates that it is modulated in the azimuthal coordinate, ϕ, by the function $\cos(2l\phi)$. Therefore, the number of intensity maxima is twice the order l of the two Bessel beams, resulting in a superposition of a lth order Bessel beam, with its mirror image, producing an intensity pattern having $2|l|$ intensity maxima, or "petals", arranged on the

circumference of the set of Bessel rings. This intensity profile experiences an angular rotation, as the field propagates along the z-axis, given by

$$\frac{d\phi}{dz} = \frac{k_{2z} - k_{1z}}{2l}. \tag{16}$$

Since the longitudinal wave vectors all propagate in different directions in the far-field and that the field contributions from the two ring-slits completely overlap (evident in Fig. 1), the angular rotation is non-zero and the entire field at P_3 experiences the rotation.

3. EXPERIMENTAL METHODOLOGY

The experimental setup used to generate superpositions of higher-order non-diffracting Bessel beams, for the investigation of the near-field ring-slit aperture, is denoted in Fig. 4. Superimposed Bessel beams were generated by illuminating a ring-slit hologram (an example is given next to LCD_1 in Fig. 4) with an expanded Gaussian laser beam ($\lambda \sim 532$ nm). The Gaussian beam was expanded through a $3 \times$ telescope and directed onto the liquid crystal display (LCD) of a SLM (HoloEye, PLUTO-VIS, with 1920×1080 pixels of pitch $8 \mu m$ and calibrated for a 2π phase shift at ~532 nm) labeled LCD_1.

The LCD was addressed with a hologram, similar to Durnin's ring-slit aperture [12], however since a phase-only SLM was used, an amplitude ring-slit was created digitally by encoding the area surrounding the ring-slit (the area which must not transmit any light) with a "checkerboard" pattern. By assigning alternating sets of pixels in the ring-slit hologram with phase values that are out of phase by π, the light reflected from LCD_1 is scattered from its initial propagation axis [16,17].

Since the "checkerboard" allows one to mimic an amplitude mask with a phase-only SLM, the azimuthal phase within the ring-slit can be addressed simultaneously in a single hologram. Assigning a single ring-slit with an azimuthal phase that varies from zero to $2\pi n$ times, a nth order Bessel beam will form in the far-field. If the ring-slit is divided into two ring-slits, where the azimuthal phase in each ring-slit varies in opposite directions (similar to that in Figs. 1 and 4) a superposition of two oppositely-handed Bessel beams will be generated. This is illustrated at the Fourier plane, P_3, of the ring-slit hologram given in Fig. 4. Here, the phase within the inner ring-slit varies three times in a clockwise direction ($l_{inner} = 3$) and three times in a counterclockwise direction ($l_{outer} = -3$) in the outer

ring-slit, thus transforming the initial Gaussian beam into a superposition of two Bessel beams, of orders $l = 3$ and -3, denoted by the "petal" structure (P_3 in Fig. 4).

More examples of ring-slit holograms are given in the top row of Fig. 5. It is not shown in the holograms, presented in Figs. 4 and 5, but in conducting the experiment, a blazed grating was added to the holograms to separate the undiffracted and diffracted components reflected from LCD_1. A diaphragm, D, was placed at the focal plane after lens L_3 to select only the first diffraction order and neglect all the other unwanted diffraction orders.

Apart from positioning a $10 \times$ objective and a CCD camera at the Fourier plane, P_3, of lens L_3, to record the non-diffracting superimposed Bessel beam, a second lens, L_4, was placed a focal length away from the Fourier plane of lens, L_3, to relay the field at LCD_1 to plane P_1. This allowed us to investigate the structure of the ring-slit field (evident at P_1) which produces a "petal" structure in the far-field (illustrated at P_3). The propagation of the ring-slit field, relayed to plane, P_1, was investigated by positioning a CCD camera on a rail and recording the field from plane P_1 to plane P_2 (a distance of two focal lengths from lens, L_4).

In the 'results' section of this paper, we will investigate the fields produced at the three different planes (P_1, P_2, and P_3) for various ring-slit holograms, as well as study the evolution of the field from plane P_1 to plane P_2, for a particular ring-slit hologram. For convenience we will refer to the Fourier transform of the ring-slit hologram (i.e., the field formed at plane P_3) as a "petal"-field. The field at the ring-slit hologram (i.e., the field at plane P_1), we will term the "singularity"-field and that formed at plane P_2 (a distance of $2f$ from lens L_4) will be termed as the "spiral"-field.

4. RESULTS AND DISCUSSION

All the digital ring-slit holograms, used in the experiment (depicted in Fig. 4), are given in the first row of Fig. 5. The first ring-slit hologram, Fig. 5(1a), consists of a single ring-slit containing an azimuthal phase of $l = +3$ and has the following dimensions (in pixels): $R_1 = 180$, $\Delta = 20$. The next five ring-slit holograms, Fig. 5(1b)–5(1f), all consist of two ring-slits, having oppositely varying azimuthal phases, varying in azimuthal order from $l_{inner} = -1$ to -5 ($l_{inner} = +1$ to $+5$), respectively. The ring-slit holograms in Figs. 5(1b)–5(1f) each have the following dimensions (in pixels): $R_1 = 180, R_2 = 190$, $\Delta = 10$. The last two ring-slit holograms [Fig. 5(1g) and 5(1h)] are divided into three and four ring-slits, respectively, having the following azimuthal orders $l_{inner} = -3$, $l_{middle} = 2$, $l_{outer} = 1$, and $l_{inner} = -2$, $l_{middle1} = -1$, $l_{middle2} = 2$, $l_{outer} = 1$.
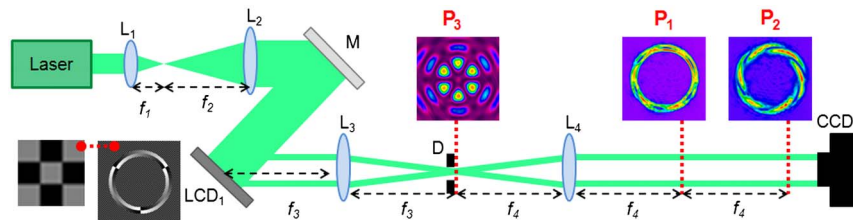

Fig. 4. (Color online) Schematic of the experimental setup for investigating the field formed by a ring-slit hologram, as well as the propagation and Fourier transform of such a field. L: lens ($f_1 = 25$ mm; $f_2 = 75$ mm; $f_3 = 100$ mm; and $f_4 = 100$ mm); M: mirror; LCD: liquid crystal display; D: diaphragm; CCD: CCD camera. The planes of interest are marked P_1, P_2, and P_3. P_3 is the Fourier plane of the ring-slit hologram; P_1 is the relayed-field (in both phase and amplitude) at the ring-slit hologram; and P_2 occurs a distance of $2f$ after L_4.
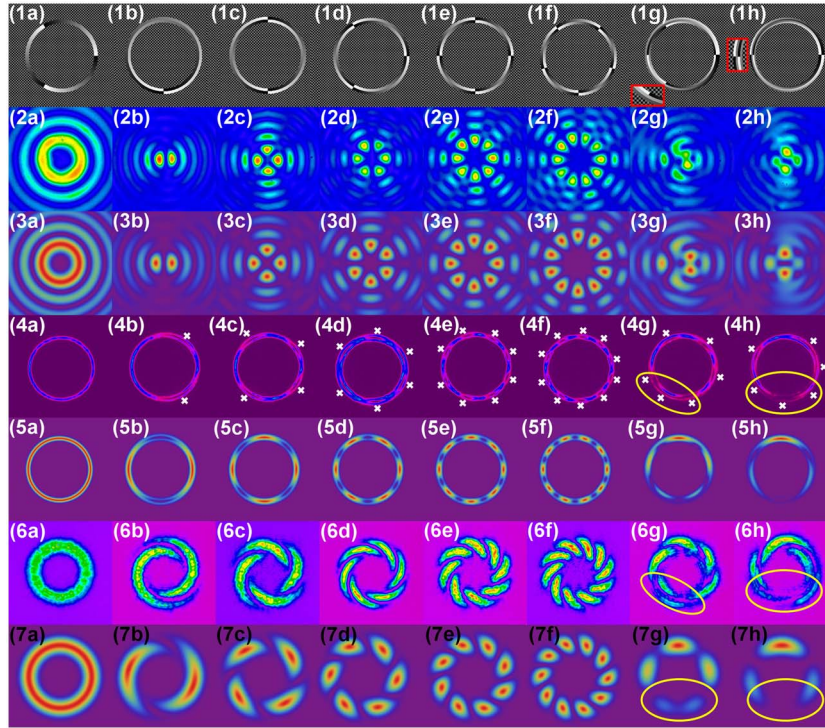
Fig. 5.   (Color online) First row: ring-slit holograms addressed to LCD_1. A zoomed-in section of three and four ring-slits are depicted as inserts (1g) and (1h). Second and third rows: experimentally produced and theoretically calculated fields produced in the Fourier plane (i.e., plane P_3), respectively. Fourth and fifth rows: experimental and theoretical fields, respectively, produced at plane P_1 (i.e., the "singularity"-fields). The white "X" marks the singularities. Sixth and seventh rows: experimental and theoretical fields, respectively, produced at plane P_2 (the "spiral"-fields).

The dimensions (in pixels) of the ring-slits in Fig. 5(1g) and 5(1h) are: $R_1 = 180$, $R_2 = 190$, $R_3 = 200$, $\Delta = 10$, and $R_1 = 168$, $R_2 = 176$, $R_3 = 184$, $R_4 = 192$, $\Delta = 8$.

The far-fields of the ring-slit holograms, presented in the first row of Fig. 5, are shown in the second row of Fig. 5, accompanied with their theoretical predictions in the third row [calculated with the use of Eq. (13)]. For a single ring-slit, containing an azimuthal index of $l = +3$, the field produced in the Fourier plane, P_3, is a third-order Bessel beam. In the case that the ring-slit hologram consists of two ring-slits, where the orders of the two azimuthal phases are of equal but opposite handedness, a "petal"-structure is produced, where the number of "petals" is denoted by $2|l|$, as expected from theory [9]. It is interesting, to note from previous investigations [9,11], that even though these fields have a global OAM of zero, their cross-sectional intensity distribution rotates as the "petal"-field propagates, due to the differing radial wave vectors. Their rotation rate, which is dependent on the differing radial wave vectors and the azimuthal index, l, is given in Eq. (16). The fields produced in the Fourier plane, P_3, for the ring-slit holograms, contained in Figs. 5(1g) and (1h) are given in Figs. 5(2g) and (2h), respectively. These two ring-slit holograms consist of three and four ring-slits, respectively, and produce a non-symmetric superposition of higher-order Bessel beams. Even though it is difficult to intuitively predict how the field will manifest in the Fourier plane for these two cases, our experimentally recorded fields (Figs. 5(2g) and 5(2h)) are in very good agreement with the theoretically calculated fields (Figs. 5(3g) and 5(3h)). These two fields are calculated by extending the amplitude distribution, given in Eq. (13), to represent a superposition of three and four Bessel beams, respectively.
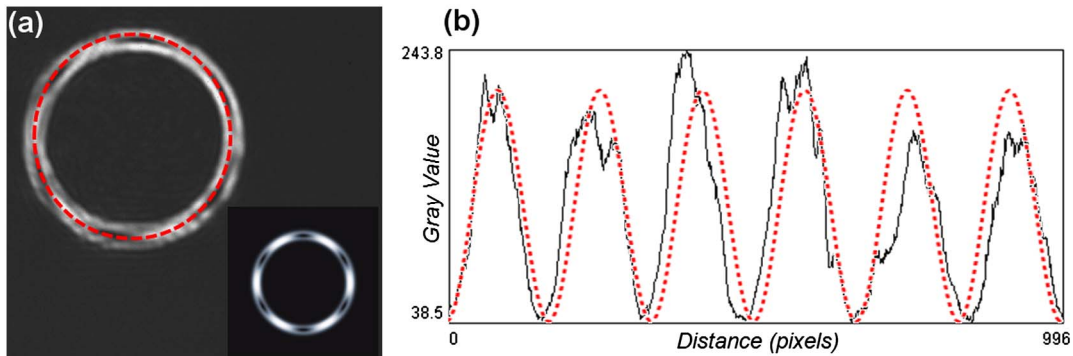

Fig. 6.   (Color online) (a) Experimentally recorded field at plane P_1 for a ring-slit consisting of the following azimuthal phases: $l_{inner} = +3$ and $l_{outer} = -3$. Theoretical prediction is given as an insert. The red, dashed ring marks the line for which the intensity profile is plotted. (b) The solid black curve is the experimental intensity profile and the red dashed curve is the theoretical intensity profile, $\cos(2l\phi)$.
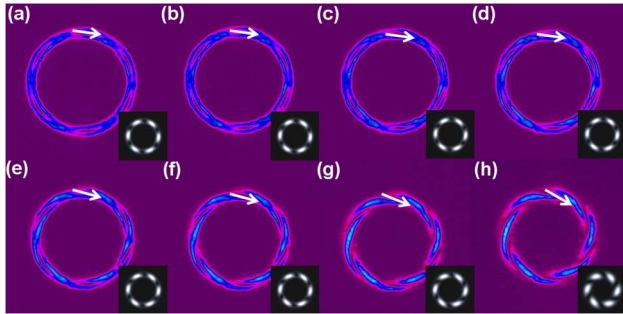
Fig. 7.   (Color online) Experimental intensity profiles of the field captured at evenly spaced intervals from plane P_1 to plane P_2. The distances from plane P_1 are given as (a) 0 mm, (b) 10 mm, (c) 20 mm, (d) 30 mm, (e) 40 mm, (f) 50 mm, (g) 60 mm, and (h) 70 mm. The white arrows illustrate the movement of a selected singularity. Inserts are given for the theoretical predictions.

The optical field produced at the plane of the ring-slit hologram (i.e., at the plane of LCD_1) was relayed to plane P_2, where all the other diffraction orders had been removed through the use of the diaphragm, D, and experimental images are shown in the fourth row of Fig. 5. It is interesting to note that when the ring-slit is addressed with a single azimuthally varying phase, no singularities appear in the ring-slit field. However, by introducing a second ring-slit (having a different radial wave-vector) singularities appear in the ring-slit field, where the number of singularities is denoted by $2|l|$ (the same for the number of "petals"). The experimental "singularity"-fields (Figs. 5(4a)–5(4f)), produced at plane P_1, are in good agreement with those predicted theoretically, using Eq. (4) (with $n = 2$) and depicted in the fifth row of Fig. 5 [Figs. 5(5a)–5(5f)]. By increasing the number of ring-slits to either three or four, it becomes very difficult to individually locate each of the singularities in the "singularity"-field as some of them start to overlap. This is evident, experimentally, within the yellow rings in Figs. 5(4g) and 5(4h) and theoretically in Figs. 5(5g) and 5(5h). Since it is difficult to locate the singularities in the "singularity"-field, when the number of ring-slits is increased, we suggest using interferometric techniques to aid the categorizing of the singularities [18].

It is well-known that the intensity of the "petal"-field is dependent on the function $\cos(2l\phi)$, evident in Eq. (15). This cosine behaviour, as a function of the azimuthal angle, of the
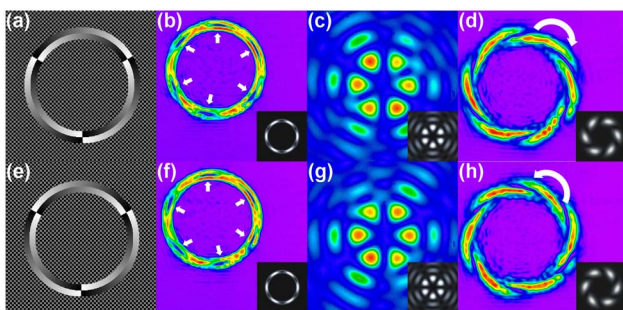

Fig. 8.   (Color online) First column: ring-slit hologram applied to LCD_1. Second column: corresponding optical fields for the ring-slits. The white arrows mark the locations of the singularities. Third column: Fourier transform of the ring-slit hologram. Fourth column: corresponding "spiral"-field, produced at plane P_2. white arrow marks the handedness of the "spokes." Theoretical predictions are accompanied as inserts.
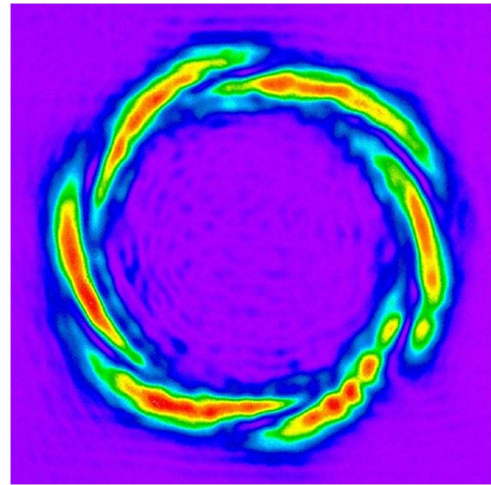

Fig. 9.   (Color online) Video clip containing experimental images for the field occurring before and after the Fourier plane for an incoming "spiral"-field produced at plane P_2 (Media 1).

intensity profile is also present in the "singularity"-field. This is evident in Fig. 6 where the intensity profile, as a function of the angular position in the field, is plotted for the "singularity"-field, for the case of $l_{inner} = +3$ and $l_{outer} = -3$. It agrees well with the intensity profile plotted for the theoretically predicted "singularity"-field, given in Eq. (6), illustrating that the intensity maxima of the near- and far-field both depend on the function $\cos(2l\phi)$.

Propagating the field a distance of one focal length from plane P_1 to plane P_2, we see that the annular structure containing singularities transforms into "spirals". The experimental fields produced at plane P_2 for each of the eight ring-slit holograms are given in the sixth row of Fig. 5 and accompanied with theoretical predictions in the seventh row. In the case of a single ring-slit, having a non-zero azimuthal mode index, the "spiral"-field appears as a diverging version of the "singularity"-field. For the five holograms, each consisting of two ring-slits, having opposite azimuthal orders, there are $2|l|$ "spokes" in the "spiral"-field, evident in Figs. 5(6b)–5(6f). Introducing more ring-slits into the hologram results in the "spokes" in the "spiral"-field to merge, making it difficult to resolve individual "spokes" (evident within the yellow rings in Figs. 5(6g), 5(6h), 5(7g), and 5(7h)).

The propagation of the "singularity"-field at plane P_1 to the "spiral"-field (at plane P_2) was recorded and selected experimental images of the field at intervals along its propagation are given in Fig. 7. It is interesting to note that even though a rotation in the intensity profile for the "petal"-field (in the vicinity of plane P_3, i.e., the far-field) exists as the "petal"-field propagates, no rotation in the "singularity"-field or "spiral"-field (i.e., near-field) exists as the field propagates. This is in accordance with the theoretical prediction given in Eq. (8), where the rotation rate for such a field is determined to be non-existent, but becomes more evident the closer the field propagates to the far-field.

Switching the handedness of the azimuthal phases in the two ring-slits, is known to cause the "petal"-field, produced in the Fourier plane, P_3, to rotate in the opposite direction [10]. Even though the "spiral"-field, produced at plane P_2, does not rotate as it propagates, swapping the handedness of the azimuthal phases (within the two ring-slits), results in the

direction of the "spokes" to switch from clockwise to counter-clockwise (and vice versa). This is evident in the last column of Fig. 8 and is in good agreement with the theoretical prediction.

Apart from investigating the appearance of the field produced by the ring-slit hologram at different propagation planes, the far-fields of the "spiral"-field (plane P_2) was also investigated and is presented as a media clip in Fig. 9. No rotation in the intensity distribution of the field before and after the existence of the non-diffracting "petal"-field is evident. The "spokes" compresses towards the propagation axis, overlapping and forming a non-diffracting "petal"-field, which exhibits a rotation in its intensity distribution as it propagates, but then the "spokes" expand outwards reconstructing the "singularity"-field.

5. CONCLUSION

In this work we have presented a class of beams which exhibit a rotation in their intensity profile in the far-field, but exhibit no rotation in the near-field. These beams are superimposed higher-order Bessel beams which are produced by encoding multiple azimuthally varying phases at different radial positions within a ring-slit aperture. We studied the field produced at the plane of the ring-slit aperture, as well as at various planes propagating from the ring-slit aperture and witnessed that the field transforms from an annular structure (embedded with singularities) to a "spiral" structure, consisting of "spokes" situated around a ring. The fields produced at the plane of the ring-slit aperture and at a distance of f from the ring-slit aperture are in good agreement with those calculated theoretically. Since Bessel beams, and especially superpositions of Bessel beams, are widely used in optical tweezing, understanding the structure of the field at planes other than the Fourier plane is necessary. The ring-slit field, embedded with singularities, can be used to trap low-index particles at set distances on the circumference of a circle. By adjusting the order, l, of the superimposed Bessel beams, one can control how many singularities are present in the ring-slit field, used to trap low-index particles. The ring-slit aperture dimensions can also be adjusted so as to control the size of the ring-slit and the distance between the singularities.

REFERENCES

1. M. W. Beijersbergen, L. Allen, H. E. L. O. Van der Veen, and J. P. Woerdman, "Astigmatic laser mode converters and the transfer of orbital angular momentum," Opt. Commun. **96**, 123–132 (1993).
2. J. Arlt and K. Dholakia, "Generation of high-order Bessel beams by use of an axicon," Opt. Commun. **177**, 297–301 (2000).
3. H. I. Sztul and R. R. Alfano, "The Poynting vector and angular momentum of Airy beams," Opt. Express **16**, 9411–9416 (2008).
4. L. Allen, M. W. Beijersbergen, R. J. C. Spreeuw, and J. P. Woerdman, "Orbital angular momentum of light and the transformation of Laguerre–Gaussian laser modes," Phys. Rev. A **45**, 8185–8189 (1992).
5. H. He, M. E. J. Friese, N. R. Heckenberg, and H. Rubinsztein-Dunlop, "Direct observation of transfer of angular momentum to absorptive particles from a laser beam with a phase singularity," Phys. Rev. Lett. **75**, 826–829 (1995).
6. A. Mair, A. Vaziri, G. Weihs, and A. Zeilinger, "Entanglement of the orbital angular momentum states of photons," Nature **412**, 313–316 (2001).
7. A. Vaziri, G. Weihs, and A. Zeilinger, "Experimental Two-Photon Three-Dimensional Quantum Entanglement," Phys. Rev. Lett. **89**, 240401–4 (2002).
8. J. T. Barreiro, T.-C. Wei, and P. G. Kwiat, "Beating the channel capacity limit for linear photonic superdense coding," Nat. Phys. **4**, 282–286 (2008).
9. R. Vasilyeu, A. Dudley, N. Khilo, and A. Forbes, "Generating superpositions of higher-order Bessel beams," Opt. Express **17**, 23389–23395 (2009).
10. R. Rop, A. Dudley, C. López-Mariscal, and A. Forbes, "Measuring the rotation rates of superpositions of higher-order Bessel beams," J. Mod. Opt. **59**, 259–267 (2011) http://dx.doi.org/10.1080/09500340.2011.631714.
11. V. V. Kotlyar, S. N. Khonina, R. V. Skidanov, and V. A. Soifer, "Rotation of laser beams with zero of the orbital angular momentum," Opt. Commun. **274**, 8–14 (2007).
12. J. Durnin, J. Miceli Jr., and J. H. Eberly, "Diffraction-free beams," Phys. Rev. Lett. **58**, 1499–1501 (1987).
13. D. McGloin, V. Garcés-Chávez, and K. Dholakia, "Interfering Bessel beams for optical micromanipulation," Opt. Lett. **28**, 657–659 (2003).
14. R. H. Jordan and D. G. Hall, "Free-space azimuthal paraxial wave equation: the azimuthal Bessel-Gauss beam solution," Opt. Lett. **19**, 427–429 (1994).
15. F. Gori, G. Guattari, and C. Padovani, "Bessel-Gauss beams," Opt. Commun. **64**, 491–495 (1987).
16. D. W. K. Wong and G. Chen, "Redistribution of the zero order by the use of a phase checkerboard pattern in computer generated holograms," Appl. Opt. **47**, 602–610 (2008).
17. A. Dudley, R. Vasilyeu, V. Belyi, N. Khilo, P. Ropot, and A. Forbes, "Controlling the evolution of nondiffracting speckle by complex amplitude modulation on a phase-only spatial light modulator," Opt. Commun. **285**, 5–12 (2012).
18. T. A. King, W. Hogervorst, N. S. Kazak, N. A. Khilo, and A. A. Ryzhevich, "Formation of higher-order Bessel light beams in biaxial crystals," Opt. Commun. **187**, 407–414 (2001).